IEEE Access
Multidisciplinary | Rapid Review | Open Access Journal

Received March 1, 2017, accepted April 6, 2017, date of publication April 18, 2017, date of current version June 7, 2017.

Digital Object Identifier 10.1109/ACCESS.2017.2695232

Gravitation-Based 3-D Redeployment Schemes for the Mobile Sensors and Sink in Gas Leakage Monitoring

HE LI, (Student Member, IEEE), YANG YANG, XUESONG QIU, (Member, IEEE), ZHIPENG GAO, AND GUIZHEN MA

State Key Laboratory of Networking and Switching Technology, Beijing University of Posts and Telecommunications, Beijing 100876, China

Corresponding author: Yang Yang (yyang@bupt.edu.cn)

This work was supported in part by the NSFC under Grant 61372108 and Grant 61401033and in part by the National Science and Technology Pillar Program under Project 2015BAI11B01.

ABSTRACT Gas leakage is one of the most frequent types of accidents in the petrochemical industry. It is imperative to use mobile sensors to monitor such an accident area. The new and effective way is to use drones and helicopters that spray wireless sensors from the air to monitor harmful gases and to locate the gas leaking source. However, the sprayed wireless sensors will be distributed randomly around the accident area, and it is a challenge to obtain effective coverage. This paper proposes a gravitation-based redeployment algorithm for sensors (GRSS) that considers the virtual boundary forces and the gas concentration in a 3-D accident monitoring area. A priority-based redeployment algorithm for sensors (PRSS) is proposed to further improve the coverage and simplify the 3-D redeployment problem. PRSS considers the layer priorities of the monitoring area to control the movements of the mobile sensors. The simulation results show that the GRSS and PRSS methods can achieve better coverage and utilize less distance compared with the random algorithm and 3-D self-deployment.

INDEX TERMS Coverage, gas leakage, mobile sensor networks, three-dimensional redeployment, virtual forces.

I. INTRODUCTION

Leaking of harmful gas could cause major personnel and property losses [1], such as those of gas leaks (December 3, 1984, Bhopal, India) or dangerous chemical explosions that involve human victims (August 12, 2015, Tianjin, China). The leaked gas could also pollute the air and harm human health. It is important to monitor the air quality of the significant areas (such as industry and residential areas) near the toxic gas that has leaked. Wireless sensor networks (WSNs) have been applied in various monitoring applications and provide an effective way to warn and avoid human victims and decrease financial losses that are caused by gas leakage incidents. In the past decade, extensive research has focused on the localization of diffusive gas leakage sources using WSNs [2]. An effective algorithm is proposed to localize a continuous gas-leakage source using the diffusion model and the information collected by the WSN [3]. A time-space domain method is proposed for gas leakage detection and locates the continuous leakage sound sources [4]. However, these algorithms focus on the localization of diffusive gas leakage sources and lack the ability to monitor the gas diffusion for the regions around the accident.

Recently, most research efforts have focused on gas WSNs [5]–[7], and there has been a growing interest in gas WSNs deployment to monitor the ambient air [8], [9]. Among these research fields, the literature [5] from the viewpoint of circuit design of gas sensors aims to avoid the zero offset issue and to select a WSN gas sensing platform that can save energy. To evaluation the performance of a gas sensor and the wireless links, a WSN (nine sensors) is deployed in a real operational boiler facility, which is aimed at the monitoring of combustible gases [6]. A novel model-based method is proposed to estimate the baseline automatically and gain the characteristics of low-cost chemical sensors while considering the temporal drift and temperature dependencies of the sensors [7]. A carbon monoxide wireless sensor network was developed to measure the carbon monoxide concentrations, and the conclusion shows that the performance and the reliability of the wireless ambient air monitoring

networks can be an alternative method for real-time air monitoring [8]. The sensors are designed and deployed on the exposed core of plastic fiber thin films of sensitive compounds to measure the low concentrations of pollutants in the atmosphere [9]. An improved artificial bee colony algorithm is designed to improve the convergence speed in an optimal deployment scheme of gas sensors [10]. A distributed air pollution sensing (APS) system is designed and implemented on wireless sensor and robot networks (WSRNs), to monitor the air quality in an urban environment by taking the energy efficiency of the sensors, the coverage of the monitoring area and the validity of the sensed data into consideration [11]. These methods all use a fixed method for the deployment of the gas sensors, and movement of the gas sensors is not considered. Thus, it is not appropriate for large-scale deployment in the region of a gas leakage accident.

The sensor nodes deployment problems in the deployment environment are divided into three categories, which include a one-dimensional line [12]–[14], 2D area [15]–[18] and 3D space [19]–[30]. The sensor networks are deployed in one-dimensional line scenarios such as river networks [12], oil pipeline networks [13] and road networks [14]. A novel geographic installation field deployment method based on a back-tracking heuristic is proposed to detect the pollutants in the river. This method considers the forks in the river, and the goal is to generate the best topology [12]. The linear sensor placement problem is used to monitor oil pipelines, and the goal is to maximize the lifetime of the sensor network [13]. The literature [14] assumes that the sensors are stochastically deployed outside the field of interest. The probabilistic expressions for k-coverage and connectivity to use the exact geometry are derived and demonstrate an on-campus traffic monitoring system using sensors along both sides of the road. Most of the sensor deployment methods are on a 2D area, and a virtual force sensor deployment algorithm is proposed to maximize the sensor field coverage [15]. To achieve k-coverage of the area, the sensor deployment problem studied is the need to minimize the number of sensors [16]. A sensor deployment strategy is proposed to avoid blindness in WSNs on the basis of ant colony optimization [17]. The literature [18] addresses this problem from both global deployment and local repairing perspectives. The enhanced virtual forces algorithm guides the sensors to their suitable positions and enhances the sensing coverage. The sensor self-organizing algorithm is used to perform local repairs in the uncovered area. For sensor deployment in 3D space, it is not appropriate to apply the 2D sensor deployment into 3D space directly [19]. Andersen and Tirthapura [20] consider the problem of deploying wireless sensors in a three-dimensional space to achieve a desired degree of coverage while minimizing the number of sensors placed. For 3D heterogeneous directional WSNs, the probabilistic expressions for k-coverage and m-connectivity are derived to optimize the cost of random deployment [22]. Some of the sensor 3D deployment methods are focused on underwater sensor deployment [23]–[26]. It is not valid to use these methods directly on the 3D surface and air deployment.

A large number of applications of WSNs utilize a 3D scenario; thus, the autonomous deployment of mobile sensors in 3D space is significant [27]. Existing solutions for mobile sensors deployment on a 3D area include [21], [28]–[30]. A decentralized random algorithm is presented to drive a group of mobile sensors on the vertices of a truncated octahedral grid for complete coverage of a bounded 3D area [28]. A distributed dynamic search coverage algorithm is proposed to search a 3D environment by using an optimal three-dimensional grid pattern for mobile WSNs [29]. In this algorithm, the mobile sensors move randomly to the vertices of the covering grid (the grid built by the mobile sensors) to perform the search task. The mobile sensors are developed to form a desired 3D geometric shape based on some consensus rules that rely only on local information. A 3D self-deployment (3DSD) algorithm to use the virtual force model is proposed to deploy the mobile WSNs [30]. This algorithm considers the negotiation tactic to ensure network connectivity and uses the density control strategy to balance the node distribution. However, selecting an appropriate sensor deployment to monitor the environments with wireless sensor networks depends on the deployment environments [21]. The gas diffusion of a leakage accident and the environment of the accident area are not considered in these algorithms, and they are not appropriate to apply directly to the monitoring of gas leakage. In this work, we design the GRSS to monitor a 3D accident area and introduce the gas concentration to improve the coverage while considering the virtual boundary force. The PRSS considers the layer priorities of the monitoring area to earn a higher coverage and support varying deployments. Compared with existing mobile 3D deployment algorithms, our proposed algorithm contributes through the following aspects:

1) The virtual boundary forces and the gas concentration are used to control the movement of sensors movement when monitor the 3D accident area. The improved methods make the sensors move to the region of greater gas concentration and limit the sensors out of the boundary.
2) The virtual sensing radius is used for the sink to prolong the network lifetime and reduce the energy holes phenomenon. The sink will increase the virtual sensing radius to leave their neighboring sensors far away when the surplus of energy in the sensors is low.
3) The monitoring area is divided into multiple layers, and the layers are defined to have different priorities. A priority-based sensor distribution algorithm for layers is proposed to redistribute the sensors that are deployed at random for each layer according to its priority.
4) To simplify the 3D redeployment problem, the monitoring area is divided into multiple layers, which changes it into multiple 2D redeployment problems. A PRSS algorithm that considers the layer priority of the

monitoring area is proposed to control the movements of the mobile sensors.

5) To prolong the network lifetime and to reduce the energy holes phenomenon, a virtual force method that considers the energy density is proposed to make the sink move into the area that has more energy.

This paper is organized as follows. Section 2 introduces the assumptions, the Gaussian Plume model and the virtual gravitation model. Section 3 describes the algorithm of GRSS. The Section 4 shows the algorithm of PRSS. Simulation results and analysis of GRSS and PRSS are presented in Section 5. Finally, the conclusions are drawn in Section 6.

II. NETWORK MODEL

A. ASSUMPTIONS

The assumptions in this paper are as follows:

1) Each sensor has the sensing range of r_s, which is much smaller than the communication range r_c. Without loss of generality, the relationship $r_c \geq 2r_s$ is assumed in our model. According to the literature [18], [31], when $r_c \geq 2r_s$, the complete coverage of a convex area implies connectivity among the working set of sensor nodes. Thus, only the sensing coverage is considered in this paper, and the network connectivity follows accordingly.
2) Each sensor and sink node can obtain its neighbor nodes' locations in its communication radius through an existing localization technique at any given time.
3) Each sensor can communicate with the sink node via a single-hop or multi-hop.
4) Each sensor can obtain the gas concentration data and will share the data with its neighboring nodes.

B. GAUSSIAN PLUME MODEL

The Gaussian plume model in the case of the wind direction, wind speed and atmospheric stability does not change with time and is defined in formula (1).

$$C(x,y,z) = \frac{q}{2\pi\sigma_y\sigma_z v_w}\exp\left(-\frac{y^2}{2\sigma_y^2}\right) * \left\{\exp\left[-\frac{(z-H)^2}{2\sigma_z^2}\right] + \exp\left[-\frac{(z+H)^2}{2\sigma_z^2}\right]\right\} \tag{1}$$

where the $C(x, y, z)$ is the gas concentration of the point (x, y, z) under the direction of the wind, q is the gas leak source release rate, H is the height of the gas leak source, v_w is the wind speed, and σ_y and σ_z are the diffusion parameter coefficients of the y and z directions, respectively. Additionally, $\sigma_y = \gamma_1 x^{\alpha 1}$ and $\sigma_z = \gamma_2 x^{\alpha 2}$, where γ_1, α_1, γ_2, and α_2 are the diffusion coefficients.

C. VIRTUAL GRAVITATION MODEL

Gravitation is one of the basic forces in nature. Gravitation means that every particle and all of the other particles attract each other. In this scheme, each sensor behaves as though it is a particle that gives a gravitational pull on the other particles. As in formula (2), the gravitation is directly proportional to the inertial mass of the two particles and is inversely proportional to the square of the Euclidean distance between the two particles.

$$F = G\frac{M_1 M_2}{R^2} \tag{2}$$

F is the gravitational force, and G is the gravitational constant. M_1 and M_2 denote the inertial mass of the two particles, and R is the Euclidean distance of the two particles. As in the application of gravitation, the experiments in the literature [32], [33] show that the R to substitute into the term R^2 can obtain better efficiency.

Given s (denoted as $s_1, s_2, \ldots, s_s$ with radius $r_{s,1}$, $r_{s,2}, \ldots, r_{s,s}$, respectively) sensors that are deployed in a 3D area, for any two sensors s_i and s_j, which are located at coordinates (x_i, y_i, z_i) and (x_j, y_j, z_j), the Euclidean distance R is $R_{ij} = ((x_i - x_j)^2 + (y_i - y_j)^2 + (z_i - z_j)^2)^{1/2}$. To make the sensors s_i and s_j not too close, the distance threshold D_{ij} is considered. If $R_{ij} < D_{ij}$, then repulsion is applied. Alternatively, if $R_{ij} > D_{ij}$, then gravitation is generated. The gravitation $\overrightarrow{F_{ij}}$ between the sensors s_i and s_j is in formula (3).

$$\overrightarrow{F_{ij}} = \begin{cases} (G_0\dfrac{C_iC_j}{R_{ij}^2}, \alpha_{ij}, \beta_{ij}, \gamma_{ij}) & R_{ij} > D_{ij} \\ 0 & R_{ij} = D_{ij} \\ (-G_0\dfrac{C_iC_j}{R_{ij}^2}, \alpha_{ij}, \beta_{ij}, \gamma_{ij}) & R_{ij} < D_{ij} \end{cases} \tag{3}$$

G_0 is the virtual gravitational constant. The parameters α_{ij}, β_{ij} and γ_{ij} are defined as the directional vectors of the force $\overrightarrow{F_{ij}}$, where $\alpha_{ij} = x_j - x_i$, $\beta_{ij} = y_j - y_i$, $\alpha_{ij} = z_j - z_i$. C_i and C_j denote the gas concentration that the two sensors s_i and s_j detected, respectively. The gas concentrations at different locations have vast differences that will lead the virtual force irrationally. Thus, the gas concentration is addressed in formula (4). Where C_s is the safe gas concentration, which is harmful to humans when the gas concentration is more than C_s.

$$C_i = \begin{cases} 1 + \ln(C_i/C_s) & C_i > C_s \\ 1 & C_i \leq C_s \end{cases} \tag{4}$$

In Fig. 1, the forces from s_j, s_l and s_k to s_i are $\overrightarrow{F_{ij}}$, $\overrightarrow{F_{il}}$ and $\overrightarrow{F_{ik}}$. This model considers the gravitation between the sensors and the sink nodes where $\overrightarrow{F_{iS}} = G_0/R_{iS}$. The force of the boundary $\overrightarrow{F_{ib}}$ is considered in this model, and $\overrightarrow{F_{ib}} = {}^x\overrightarrow{F_{ib}} + {}^y\overrightarrow{F_{ib}} + {}^z\overrightarrow{F_{ib}}$. Where ${}^x\overrightarrow{F_{ib}} = G_0/{}^xR_{ib}$, ${}^y\overrightarrow{F_{ib}} = G_0/{}^yR_{ib}$ and ${}^z\overrightarrow{F_{ib}} = G_0C_i/{}^zR_{ib}$. The boundary is defined the location that the gas concentration is C_s. The distances between the sensor i and the boundary from the x, y and z axis are ${}^xR_{ib}$, ${}^yR_{ib}$ and ${}^zR_{ib}$. The boundary coordinates along the x, y and z axis of sensor i can be obtained by solving the equation $C(x_{i,b}, y_i, z_i) = C_s$, $C(x_i, y_{i,b}, z_i) = C_s$ and

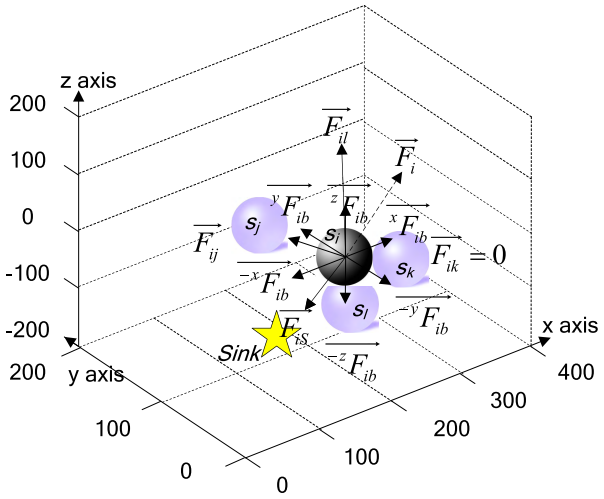

FIGURE 1. The gravitation on the sensor s_i.

$C(x_i, y_i, z_{i,b}) = C_s$. The distances ${}^xR_{ib}$, ${}^yR_{ib}$ and ${}^zR_{ib}$ can be calculated by ${}^xR_{ib} = |x_i - x_{i,b}|$, ${}^yR_{ib} = |y_i - y_{i,b}|$ and ${}^zR_{ib} = |z_i - z_{i,b}|$. The resultant force $\overrightarrow{F_i}$ is considered to be the gravitation and repulsion, which can be extended on s_i and defined as in formula (5). The sensor s_i will move to the next position according to $\overrightarrow{F_i}$. The $(\alpha_i, \beta_i, \gamma_i)$ is the directional moving vector of $\overrightarrow{F_i}$ in Fig. 1. The acceleration of sensor i at time t is defined as in formula (6).

$$\overrightarrow{F_i} = \overrightarrow{F_{iS}} + \overrightarrow{F_{ib}} + \sum_{j=1,j\neq i}^{s} \overrightarrow{F_{ij}} \tag{5}$$

$$\overrightarrow{a_{ij}} = \overrightarrow{F_{ij}}/C_i \tag{6}$$

FIGURE 2. The distance threshold D_{ij} settings in two different conditions: (a) when $\delta \leq 1$ and (b) when $\delta > 1$.

III. GRAVITY-BASED REDEPLOYMENT ALGORITHM

A. DISTANCE THRESHOLD

The distance threshold is the overlap degree of the two sensors. The distance threshold is used to keep the overlap level reasonably. The value of the distance threshold depends on the sensor density. Assuming that the target area size is V, the sensing radius of sensor i is r_i, the number of sensors in the target area is n, and the sensing area size of all of the sensors is defined as V_s, where $V_s = 4\pi/3 \sum_{i=1}^{n} r_i^3$. The δ is defined as the maximum possible coverage ratio, and $\delta = V_s/V$. In Fig. 2, the two different conditions between any two sensors s_i and s_j are introduced to design the distance threshold D_{ij}. Fig. 2(a) shows that the sensors are not sufficient to cover the target area ($\delta \leq 1$). Fig. 2(b) shows that the sensors are sufficient to cover the target area and allows a certain degree of overlap ($\delta > 1$). The distance threshold D_{ij} in this scheme is defined as in formula (7).

$$D_{ij} = \begin{cases} r_i + r_j & \delta \leq 1 \\ (r_i + r_j)/\delta & \delta > 1 \end{cases} \tag{7}$$

B. ADDRESSING THE SINK NODE

In the WSNs, the sink node is used to collect the sensing information of the sensors. The data of the sensors are sent to the sink nodes by a multi-hop. The sensors nearby the sink not only transmit their own generated data but also forward the other nodes' data. The sensors near the sink will transmit many more data packets than the sensors that are far away from the sink, and thus, it is easy for the sink nodes to produce energy holes in the WSNs. To prolong the network lifetime and to avoid the energy holes phenomenon, the virtual sensing radius method is used for a sink to make the network nodes load balancing.

The surplus energy of sensor i is defined as ε_i, and the communication radius of sensor i is $r_{c,i}$. The sensors will send their surplus energy ε_i to the sink node when they send the collected data. The sink will calculate the average surplus energy after it receives all of the surplus energy of the WSNs. The average surplus energy ε_A can be calculated as $\varepsilon_A = \sum_{i=1}^{n} \varepsilon_i/n$. The sink will increase the virtual sensing radius to leave the neighboring sensors i away from it when the surplus energy $\varepsilon_{i,sink}$ of the sensor i near the sink is lower than the average surplus energy ε_A. Fig. 3(a) shows the forces of sensor i when the sensor network is stable. The resultant forces of sensor i from the sensors s_j, s_k and the sink is zero. Fig. 3(b) shows the forces of sensor i when the sink increases $r_{s,sink}$ and breaks the force balance of sensor i. The sink increases $r_{s,sink}$ in such a way that the distance threshold between the sink and sensor i becomes $D_{is} = \delta\,(r_i + r_{s,sink})$. However, the distance $R_{i,sink}$ between the sink and sensor i is not changed, and the repulsion will be generated to s_i because $R_{i,sink} < D_{is}$. Then, sensor i will leave and go away from the sink. The $r_{s,sink}$ of the sink is only used for its neighboring sensor i and sets $r_{s,sink} = r_{s,i}$.

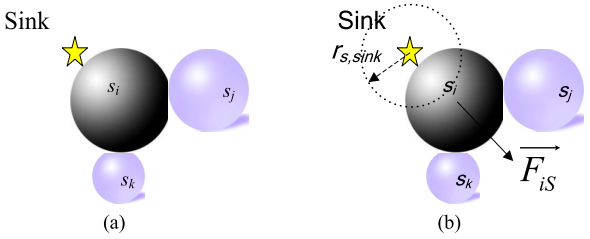

FIGURE 3. The force of the sink uses the virtual sensing radius: (a) The force of sensor i when $r_{s,sink} = 0$; (b) The force of sensor i when $r_{s,sink} > 0$.

C. GRSS ALGORITHM SUMMARY

To reduce the energy consumption of the sensors on the movements, $L_{max,i}$ is defined as the maximum movement

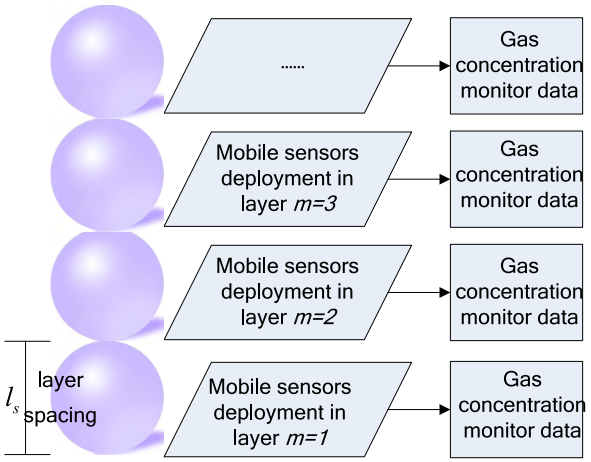

FIGURE 4. The monitoring area divided into multiple layers to deploy.

length to limit the movement of the sensors. First, each sensor calculates $\overrightarrow{F_i}$ and the movement distance $l_i = a_{ij}\Delta_t^2/2$ according to its location and the update time Δ_t, where Δ_t is the interval time for the sensors to calculate their new virtual force. Sensor i can calculate the sum of the movement distance $L_{Sum,i}$ at time t. Then, the sensor will move to the next position when $\overrightarrow{F_i} \neq 0$. Finally, if $\varepsilon_{i,sink} \leq \varepsilon_A$, the sink sets $r_{s,sink} = r_{s,i}$ and notifies the neighboring sensors, which breaks the force balance of sensor i. When $L_{Sum,i} \geq L_{max,i}$, the GRSS algorithm is terminated.

Algorithm 1 Gravity-Based Redeployment for the Sensors and Sink (GRSS)

Initialize set $L_{Sum,i} = 0$, $r_{s,sink} = 0$;
while $(L_{Sum,i} < L_{max,i})$ **do**
  if $(\varepsilon_{i,sink} \leq \varepsilon_A)$ **do**
    the sink sets $r_{s,sink} = r_{s,i}$ and notifies its neighboring sensors;
  end if
    for each sensors $s_i \in S = \{s_1, s_2, .., s_s\}$ **do**
      Calculate $\overrightarrow{F_i}$, l_i;
    end for
      if $(\overrightarrow{F_i} \neq 0)$ **do**
        the sensors s_i move to the next positions;
      end if
        update the sum of the movement distances $L_{Sum,i}$;
end while

IV. PRIORITY-BASED REDEPLOYMENT ALGORITHM

A. PRIORITY OF EACH LAYER

The layered structure of the monitoring area is shown in Fig. 4. The monitoring area is divided into multiple layers. The 3D sensors redeployment problem in gas leakage monitoring is changed into 2D. The layers of the monitoring area and the gas leak source are defined to have different priorities. The priority function is defined as in formula (8).

$$\varphi(m) = \begin{cases} 1 & m = \lceil H/l_s \rceil \\ e^{-|m-\lceil H/l_s \rceil|} & else \end{cases} \tag{8}$$

$\varphi(m)$ is the priority function of the layer m of the monitoring area, where m is the layer number of the monitoring area from the bottom up and can be calculated as $m = \lceil z/r_a \rceil$; z is the height of the layer on which the sensors will be deployed; l_s is the layer spacing between the two adjacent layers of the monitoring area, where $l_s = z/\lceil z/r_a \rceil$; and $r_a = \sum_{i=1}^{n} r_i/n$. The location of the gas leak source has been solved by diffusion-based parallel and sequential projection methods [34], and the H can be obtained. The monitoring area of the gas leak source is important; thus, the priority is the highest and is set to 1 in formula (8).

B. DISTRIBUTION OF SENSORS

In Fig. 4, when the monitoring area is large, the sensors might not always be sufficient to cover all of the area. The deployed sensors should be redistributed to the layers according to the priorities. Each layer distribution of sensors is defined as in formula (9).

$$n_m = \left[n * \varphi(m) \Big/ \sum_{m=1}^{n} \varphi(m) \right] \tag{9}$$

Where n_m is the number of sensors distributed in the m layer, and $n = \sum_{m=1}^{m} n_m$. The higher the layer priority, the more sensors will be distributed and deployed in the layer. The distribution of sensors is described in algorithm 2. First, the sensors are deployed at random and should establish a communication connection with one another and confirm the layer that the sensor is in. Then, the sensors in layer m calculate the number of sensors n_m that should be distributed according to formula (9) and count the real number of sensors n'_m. If the real number of sensors n'_m in layer m is more than n_m, then the $n'_m - n_m$ (if $n'_m - n_m \leq n'_{m-1} - n_{m-1}$) or $n'_{m-1} - n_{m-1}$ (if $n'_m - n_m > n'_{m-1} - n_{m-1}$) sensors near layer $m - 1$ will be selected and move into layer $m - 1$ when $n'_{m-1} \leq n_{m-1}$ and $(\varphi(m-1) > \varphi(m+1))$. If $n'_{m-1} \geq n_{m-1}$ or $\varphi(m-1) < \varphi(m+1)$, then $n'_m - n_m$ (if $n'_m - n_m \leq n'_{m+1} - n_{m+1}$) or $n'_{m+1} - n_{m+1}$ (if $n'_m - n_m > n'_{m+1} - n_{m+1}$) sensors near layer $m + 1$ will move into layer $m+1$. If the real number of sensors n'_m in layer m is less than n_m, then these sensors will wait for the sensors of its adjacent layers to move to layer m.

C. REDEPLOYMENT OF SENSORS IN EACH LAYER

In this model, the gravitational force exists only in the same layer. Given ${}^mS$ (denoted as ${}^ms_1, {}^ms_2, \ldots, {}^ms_s$ with radius ${}^mr_{s,1}, {}^mr_{s,2}, \ldots, {}^mr_{s,s}$, respectively) sensors deployed in the layer m monitoring area, any two sensors ms_i and ${}^ms_j$ are located at coordinates $({}^mx_i, {}^my_i)$ and $({}^mx_j, {}^my_j)$, and $R_{ij} = (({}^mx_i - {}^mx_j)^2 + ({}^my_i - {}^my_j)^2)^{1/2}$. We make the sensors ${}^ms_i$ and ${}^ms_j$ not too close to enable the distance threshold ${}^mD_{ij}$ to

Algorithm 2 Priority-Based Sensor Distribution for the Layers (PSDL)

1: **Initialize** set $n'_m = 0$, $n_m = 0$;
2: Each sensor in layer m calculates n_m;
3: Each sensor in layer m counts n'_m;
4: **while** $(n'_m \neq n_m)$ **do**
5: **if** $(n'_m > n_m)$ **do**
6: **if** $((n'_{m-1} \leq n_{m-1})\&\&(\varphi\ (m\text{-}1) > \varphi\ (m\text{+}1)))$ **do**
7: **if** $((n'_m\text{-}n_m) \leq (n'_{m-1}\text{-}n_{m-1}))$ **do**
8: Select $(n'_m\text{-}n_m)$ sensors near layer *m-1*;
The selected sensors are moving into layer *m-1*;
9 **end if**
10: Select $(n'_{m-1}\text{-}n_{m-1})$ sensors near layer *m-1*;
The selected sensors are moving into layer *m-1*;
11: **end if**
12: **if** $(n'_{m+1} \leq n_{m+1})$ **do**
13: **if** $((n'_m\text{-}n_m) \leq (n'_{m+1}\text{-}n_{m+1}))$ **do**
14: Select $(n'_m\text{-}n_m)$ sensors near layer *m+1*;
The selected sensors are moving into layer *m+1*;
15 **end if**
16: Select $(n'_{m+1}\text{-}n_{m+1})$ sensors near layer *m+1*;
The selected sensors are moving into layer *m+1*;
17: **end if**
18: **end if**
19: Each s_i updates the n'_m of its layer;
20: **end while**

also be used in each layer. If ${}^mR_{ij} < {}^mD_{ij}$, then repulsion is applied. Additionally, if ${}^mR_{ij} > {}^mD_{ij}$, then gravitation will be generated. The gravitation between sensors ${}^ms_i$ and ${}^ms_j$ is defined as in formula (10). ${}^mC_i$ and ${}^mC_j$, respectively, denote the unit gas concentrations of the two sensors ${}^ms_i$ and ${}^ms_j$. G_0 is the gravitational constant.

$$\overrightarrow{{}^mF_{ij}} = \begin{cases} (G_0 \dfrac{{}^mC_i\,{}^mC_j}{{}^mR_{ij}}, {}^m\theta_{ij}) & {}^mR_{ij} > {}^mD_{ij} \\ 0 & {}^mR_{ij} = {}^mD_{ij} \\ (-G_0 \dfrac{{}^mC_i\,{}^mC_j}{{}^mR_{ij}}, {}^m\theta_{ij} + \pi) & {}^mR_{ij} < {}^mD_{ij} \end{cases} \quad (10)$$

The ${}^m\theta_{ij}$ is defined as the direction of the force $\overrightarrow{{}^mF_{ij}}$, and ${}^m\theta_{ij}$ can be calculated in formula (11).

$${}^m\theta_{ij} = \tan^{-1} \frac{({}^my_i - {}^my_j)}{({}^mx_i - {}^mx_j)} \quad (11)$$

In Fig. 5, the gravitation from ${}^ms_j$ to ${}^ms_i$ is $\overrightarrow{{}^mF_{ij}}$, and the repulsion from ${}^ms_k$ (it is close to ${}^ms_i$) to ${}^ms_i$ is $\overrightarrow{{}^mF_{ik}}$. The gravitation from ${}^ms_l$ to ${}^ms_i$ is $\overrightarrow{{}^mF_{il}} = 0$, which means that there is no force on ${}^ms_i$ from ${}^ms_l$. This model considers the gravitation $\overrightarrow{{}^mF_{iS}}$ between the sensors and the sink nodes,

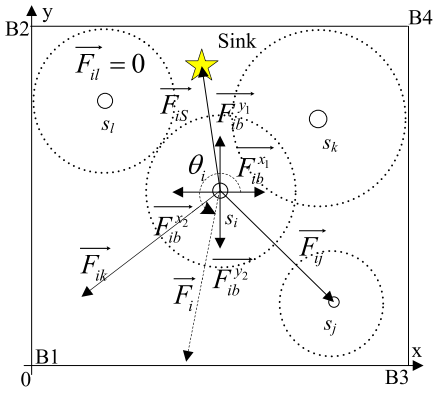

FIGURE 5. The gravitation on a sensor ${}^ms_i$ in the layer *m* area.

where $\overrightarrow{{}^mF_{iS}} = G_0/{}^mR_{iS}$. The force of the boundary $\overrightarrow{{}^mF_{ib}}$ is also used in this model, where $\overrightarrow{{}^mF_{ib}} = G_0/{}^mR_{ib}$. The boundary coordinates along the x and y axis of sensor ${}^ms_i$ can be obtained by solving the equation $C({}^mx_{i,b}, {}^my_i, {}^mz_i) = C_s$ and $C({}^mx_i, {}^my_{i,b}, {}^mz_i) = C_s$. The distances between the sensor ${}^ms_i$ and the boundary from the x and y axis ${}^{x,m}R_{ib}$ and ${}^{y,m}R_{ib}$ can be calculated by ${}^{x,m}R_{ib} = |{}^mx_i - {}^mx_{i,b}|$ and ${}^{y,m}R_{ib} = |{}^my_i - {}^my_{i,b}|$. The gravitation and the repulsion are considered in that the resultant force $\overrightarrow{{}^mF_i}$ can be extended on ${}^ms_i$ as in formula (12).

$$\overrightarrow{{}^mF_i} = \overrightarrow{{}^mF_{iS}} + \overrightarrow{{}^mF_{ib}} + \sum_{j=1, j\neq i}^{s} \overrightarrow{{}^mF_{ij}} \quad (12)$$

Sensor ${}^ms_i$ will move to the next position according to $\overrightarrow{{}^mF_{ik}}$. The ${}^m\theta_i$ is the moving direction angle of the sensor ${}^ms_i$, as given in Fig. 5. The acceleration of the sensor ${}^ms_i$ at time t is defined as $\overrightarrow{{}^ma_{i,t}} = \overrightarrow{{}^mF_i}/{}^mC_i$.

D. DISTANCE THRESHOLD OF EACH LAYER AREA

Similar to the above description, the value of the distance threshold of each layer area also depends on the sensor density. Assume that the m layer monitoring area size is ${}^mA$ and the sensing area size of all of the sensors is defined as ${}^mA_s$, where ${}^mA_s = \sum_{i=1}^{n_m} \pi {}^mr_i^2$. The ${}^m\delta$ is defined as the maximum possible coverage ratio, where $r{}^m\delta = {}^mA_s/{}^mA$. The coverage ratio ${}^m\delta \leq 1$ means that the sensors are not sufficient to cover the layer m monitoring area and thus to maximize the coverage area, overlap is not allowed between the sensors. On the other hand, if the coverage ratio has ${}^m\delta > 1$, then the sensors are sufficient to cover the layer m monitoring area. In other words, the sensors can allow a certain degree of overlap. In Fig. 6, the two different conditions between any two sensors ${}^ms_i$ and ${}^ms_j$ are introduced to design the distance threshold ${}^mD_{ij}$. Fig. 6(a) shows that the sensors are not sufficient to cover the target area (${}^m\delta \leq 1$), and ${}^mD_{ij} = {}^mr_i + {}^mr_j$. It is sufficient to allow a certain degree of overlap in Fig. 6(b) (${}^m\delta > 1$), and ${}^mD_{ij} = ({}^mr_i + {}^mr_j)/{}^m\delta$.

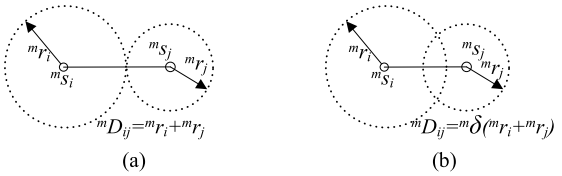

FIGURE 6. The distance threshold ${}^{m}D_{ij}$ settings under two different conditions: (a) The distance threshold ${}^{m}D_{ij}$ settings when the coverage ratio ${}^{m}\delta \leq 1$; (b) The distance threshold ${}^{m}D_{ij}$ settings when the coverage ratio is ${}^{m}\delta > 1$.

E. REDEPLOYMENT OF THE MOBILE SINK NODE

The target to address the sink node in the GRSS algorithm is to reduce the energy holes phenomenon through sensor redeployment. However, this method uses the virtual sensing radius of the sink, which will produce the sensing hole, and the sink is static while the ability to prolong the network lifetime is limited. To prolong the network lifetime and to avoid the energy holes phenomenon, a dynamic method is proposed to make the sink to move according to the energy density. Assume that S_P (denoted as $s_1, s_2, \ldots, s_p$ with radius $r_{s,1}, r_{s,2}, \ldots, r_{s,p}$, respectively) sensors are in the sink node's 3D communication area. The energy density is defined as in formula (13).

$$\rho_s = 3\sum_{i=1}^{p} \varepsilon_i / 4\pi r_{c,sink}^3 \tag{13}$$

Where ρ_s is the energy density in the communication area of the sink, ε_i is the surplus energy of sensor i in the communication area of the sink, and $r_{c,sink}$ is the communication radius of the sink.

$$\rho_i = 3(\varepsilon_i + \sum_{j=1}^{n_i} \varepsilon_{j,i}) / 4\pi r_{c,i}^3 \tag{14}$$

Where ρ_i is the energy density in the communication area of sensor i, n_i is the number of sensors in the communication area of sensor i, ε_{ij} is the surplus energy of sensor j in the communication area of sensor i, and $r_{c,i}$ is the communication radius of sensor i. The sensors near the sink will send their ρ_i to the sink node when sending the collected data. Thus, the force $\overrightarrow{F_{S,i}}$ of the sink from the sensor i nearest the sink is given in formula (15):

$$\overrightarrow{F_{S,i}} = \begin{cases} (G_0 \varepsilon_i / R_{S,i}, \alpha_{S,i}, \beta_{S,i}, \gamma_{S,i}) & \rho_S < \overline{\rho} \text{or} \rho_S < \rho_i \\ 0 & \rho_S \geq \rho_i \end{cases} \tag{15}$$

Where the $\alpha_{S,i}$, $\beta_{S,i}$ and $\gamma_{S,i}$ are defined as the direction vectors of the force $\overrightarrow{F_{S,i}}$. The average energy density $\overline{\rho}$ is calculated as $\overline{\rho} = \sum_{m=1}^{m} (\sum_{i=1}^{n_m} \rho_i / n_m)$. In Fig. 7, the gravitation from s_i, s_j and s_k to the sink is $\overrightarrow{F_{S,i}}$, $\overrightarrow{F_{S,j}}$ and $\overrightarrow{F_{S,k}}$, respectively. Thus, the resultant force $\overrightarrow{F_S}$ can be calculated as $\overrightarrow{F_S} = \overrightarrow{F_{S,i}} + \overrightarrow{F_{S,j}} + \overrightarrow{F_{S,k}}$. The sink will move to the next position according to $\overrightarrow{F_S}$ when the force is not zero. The acceleration of the sink at time t is defined as $\overrightarrow{a_{S,t}} = \overrightarrow{F_S} / \varepsilon_i$.

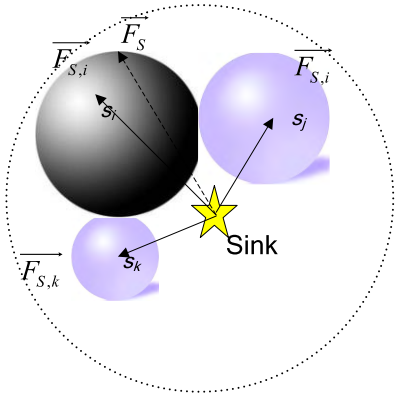

FIGURE 7. The force of the sink from the nearby sensors.

F. ENERGY CONSUMPTION MODEL

Here, we consider the radio model and the related parameters referenced in the literature [35]. The energy consumption of each sensor node sends a packet to the next forwarding node over a distance r_c, which is defined as in formula (16).

$$E_T(l, r) = le_{elec} + l\varepsilon_{fs} r_c^2 \tag{16}$$

The energy consumption of each sensor node receives a packet as in formula (17).

$$E_R(l) = le_{elec} \tag{17}$$

Where l is the packet length, e_{elec} is the energy consumption of the electronic equipment of 1 bit, and ε_{fs} is the energy consumption of the wireless antenna amplifier. Thus, the energy consumption of i to relay a packet one time is defined as in formula (18).

$$E_i = E_{T,i}(l, r_c) + E_R(l) \tag{18}$$

G. PRSS ALGORITHM SUMMARY

To reduce the energy consumption of the sensors, the value of ${}^{m}L_{max,i}$ is the maximum movement length, to limit the movement of the sensors. First, the sensors can be deployed at random, and the sensors must be distributed according to algorithm 2. If the real number of sensors n'_m in layer m is less or more than n_m, then the sensors in the adjacent layer will move to layer m, or the redundant sensors will move to the other layers. Then, the sensors of every layer calculate the virtual forces ${}^{m}\overrightarrow{F_i}$, $\overrightarrow{F_S}$ and the movement distance ${}^{m}l_i = {}^{m}a_{ij}\Delta_t^2/2$ according to their location at each Δ_t. The sensor i can calculate the sum of the movement distance ${}^{m}L_{Sum,i}$ at time t. Finally, if ${}^{m}\overrightarrow{F_i} \neq 0$, then the sensors will move to the next positions. When ${}^{m}L_{Sum,i} \geq {}^{m}L_{max,i}$, then the redeployment of sensor i is terminated. As in the sensor redeployment, $L_{max,S}$ is defined as the maximum movement length to limit the movement of the sink. The sink can calculate the movement distance easily according to the location at each Δ_t, and $L_{Sum,S}$ can be calculated easily. When $L_{Sum,S} \geq L_{max,S}$, the redeployment of the sink is terminated.

The difference between the GRSS and PRSS is that the PRSS does not allow any movement between the layers after the sensor nodes are redistributed between the layers. This method can guarantee that the layers of high priority have enough sensors to monitor. The PRSS is suitable for application in a situation in which the monitoring area is large and the number of sensors is not sufficient to monitor the whole area. In contrast, the GRSS is appropriate to use in the small area and has plenty of sensors.

Algorithm 3 Priority-Based Redeployment for the Sensors and Sink (PRSS)

Initialize set ${}^{m}L_{Sum,i} = 0$, $r_{s,sink} = 0$, $L_{Sum,S} = 0$;
  while $({}^{m}L_{Sum,i} <^{m} L_{max,i}) || (L_{Sum,S} < L_{max,S})$ **do**
    for the sink and each sensor ${}^{m}s_i \in {}^{m}S = \{{}^{m}s_1, {}^{m}s_2, .., {}^{m}s_s\}$ **do**
      the sensor ${}^{m}s_i$ and sink calculate $\overrightarrow{{}^{m}F_i}$, $\overrightarrow{F_S}$ respectively;
    end for
    if $(\overrightarrow{{}^{m}F_i} \neq 0)$ **do**
      the sensors ${}^{m}s_i$ move to the next positions;
    end if
      update the sum of the movement distances ${}^{m}L_{Sum,i}$;
      if $(\overrightarrow{F_S} \neq 0)$ **do**
      the sink moves to the next position;
      end if
      update the sum of the movement distances ${}^{m}L_{Sum,S}$;
  end while

V. SIMULATION RESULTS AND ANALYSIS

In this section, the proposed GRSS and PRSS protocols are validated by comparing their performances with other self-deployment mechanisms in terms of the coverage ratio, movement distance, energy consumption and network lifetime, by sensor physical movements. For 3D deployments, we deploy the sensor nodes randomly at the beginning and implement the 3DSD mechanisms, GRSS (improved virtual forces mechanism considered the boundary forces and the gas concentration) and PRSS (improved GRSS mechanism considered the priority of the layer in the monitoring area).

There is a sink node to collect the data in our simulation model. In the communication simulation, the MAC protocol of ZigBee is 128 kbps 802.15.4. The communication energy parameters are set as $e_{elec} = 50$ μJ/bit, $\varepsilon_{fs} =$ 10 nJ/bit. To assess the performance of the proposed scheme, a 100 m×100 m×100 m 3D area is selected to deploy the mobile sensors. The speeds of the mobile sensors v_j are between 0 m/s and 5 m/s. The communication radius of the sensor i is $r_{c,i} = 30$ m, and the sensing radius of the sensor i is $r_{s,i} = 15$ m. The initial energy of all of the sensors is set to $\varepsilon_0 = 1000$ Joules, and the data transfer rate is $r_{t,i} = 128$ kbps. The data size of s_i collected at unit time is $D_i = 128$ bit/s, and the packet length of the sensor is $l = 256$ bit. The detailed simulation parameters are shown in Table I.

TABLE 1. Simulation parameters.

Symbol	Parameter	value
$r_{t,i}$	Transmission rate of Zigbee	128 kbps
r_s	The sensing radius	15 m
$r_{s,sink}$	The virtual sensing radius of the sink	15 m
r_c	The communication radius	30 m
$L_{max,S}$	The maximum movement length	1000 m
l	The packet length of the sensor	256 bit
D_i	The data size of the sensors collected at unit time	128 bit/s
e_{elec}	The energy consumption of the electronic equipment of 1 bit	50 μJ/bit
ε_{fs}	The energy consumption of the wireless antenna amplifier	10 nJ/bit
ε_0	The initial energy of all of the sensors	1000 J
G_0	The gravitational constant	10.0
C_s	The gas safe concentration	10^{-9}kg/m^3

A. SIMULATION OF GAUSSIAN GAS DIFFUSION IN THE MONITORING AREA

According to the above plume model, the simulation of gas diffusion is built first as in Fig. 8. The location of the gas leak source is the origin; the x-axis denotes the distance downwind, the y-axis denotes the distance crosswind, and the z-axis denotes the gas diffusion concentration. The height of the gas leak source $H = 80.0$ m, the gas leak source release rate $q = 30.0$ mg/s, and the wind speed $v_w = 1.0$ m/s. The horizontal diffusion coefficients are $\gamma_1 = 0.1107$, $\alpha_1 = 0.9500$. The vertical diffusion coefficients are $\gamma_2 = 0.1046$, $\alpha_2 = 0.9200$. The gas simulation diffusion is at different heights, and in Fig. 8, a large number of points on the surface at the different heights are selected to obtain the corresponding concentration.

The gas concentration is the lowest when the height is 12.5 m, as shown in Fig. 8. The reason is that the horizontal area at 12.5 m is far away from the gas leak source. The area of higher gas concentration is at the border downwind, as in Fig. 8(a). When the height is 37.5 m, the gas concentration distribution is similar to that in Fig. 8(a). However, the gas concentration at 37.5 m is approximately 10 orders of magnitude more than in the monitoring area at z=12.5 m. This finding is because the monitoring area at 37.5 m is much nearer to the gas leak source than at 12.5 m. The monitoring area at 62.5 m is much nearer to the gas leak source than at 12.5 m and 37.5 m in Fig. 8(c). Thus, the gas concentration at 62.5 m is approximately 17 orders of magnitude more than at 12.5 m and is approximately 6 orders of magnitude more than at 37.5 m. When the height is 87.5 m, the gas concentration distribution is the highest of the four different heights. The simulation of the gas diffusion shows that the different heights have great differences. The gas concentration of the horizontal area at the same height also has a large difference. Thus, it is necessary to consider the gas concentration and the

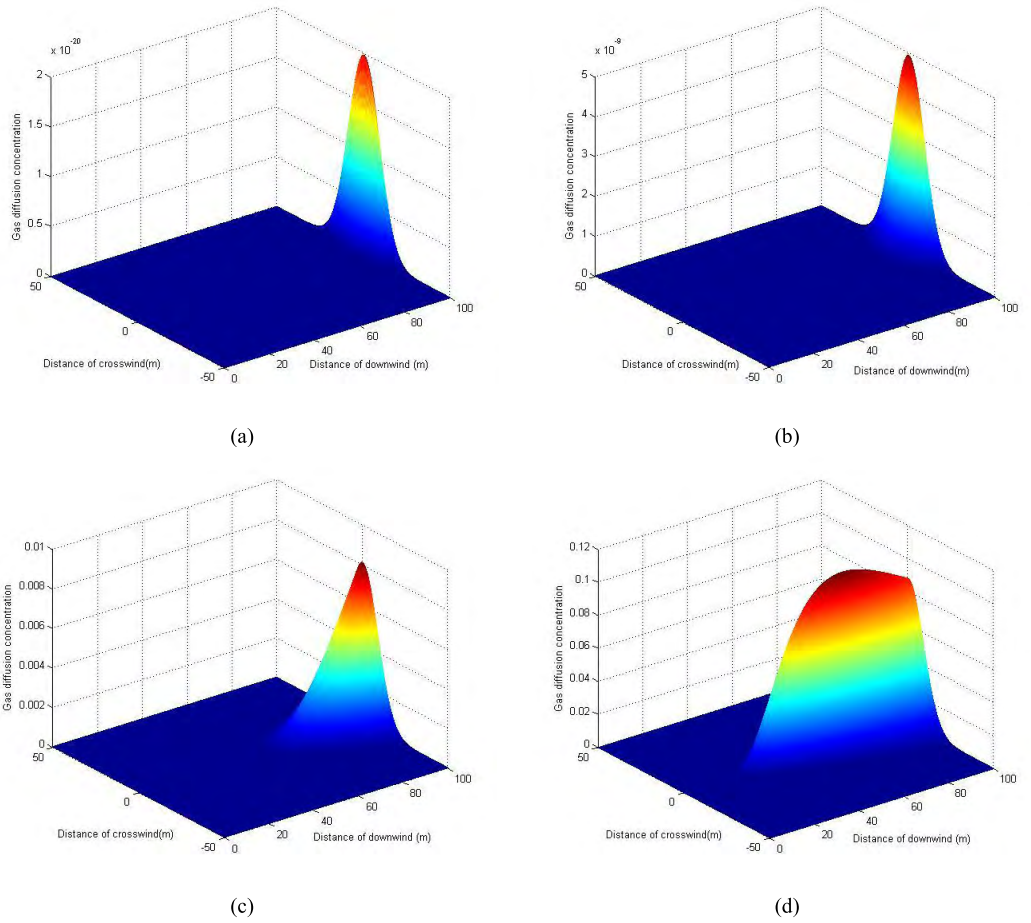

FIGURE 8. The gas simulation diffusion at four different heights: (a) the gas simulation diffusion when $z = 12.5$ m; (b) the gas simulation diffusion when $z = 37.5$ m; (c) the gas simulation diffusion when $z = 62.5$ m; and (d) the gas simulation diffusion when $z = 87.5$ m.

priority of the monitoring area when deploying the mobile sensors.

B. SIMULATION OF THE COVERAGE

For a 3D sensing environment, the network typically starts with a random deployment of sensor nodes. Fig. 9(a) displays the deployment results of 50 sensors scattered over the area ($\delta < 1$) using RAND, 3DSD, GRSS and PRSS at the 50^{th} round, and Fig. 9(b) displays the deployment results of 100 sensors scattered over the area ($\delta > 1$) using RAND, 3DSD, GRSS and PRSS at the 100^{th} round. The maximum possible coverage ratio $\delta = 0.7069$ is set for the algorithm RAND, 3DSD, GRSS and PRSS in Fig. 9(a). The maximum possible coverage ratios of every layer in the monitoring area are ${}^1\delta = 0.8149$, ${}^2\delta = 0.5432$, ${}^3\delta = 0.7069$, and ${}^4\delta = 0.8149$, respectively. The maximum possible coverage ratio $\delta = 1.4137$ is set for the algorithms RAND, 3DSD, GRSS and PRSS in Fig. 9(b). The maximum possible coverage ratios of every layer in the monitoring area are ${}^1\delta = 1.4667$, ${}^2\delta = 1.2494$, ${}^3\delta = 1.2494$, and ${}^4\delta = 1.4667$, respectively. The monitoring area of the first layer near the ground is important for humans and thus we also define the priority as 1.

From Fig. 9, PRSS is the most effective sensing coverage at the same round. 3DSD make some of the sensors out of the sensing area due to a lack of boundary forces. The GRSS can avoid the unnecessary movements that make sensors maintain a certain distance from the boundary because of the boundary forces. Thus, compared with 3DSD, the coverage ratio of GRSS is higher than 3DSD. The sensor distributions of GRSS (Figs. 9(a3) and 9(b3)) are relatively central compared with 3DSD (Fig. 9(a2) and Fig. 9(b2)) because the gas concentration is considered in the GRSS. However, due to the layer structure, PRSS makes some of the sensors be out of the sensing area. Thus, the coverage ratio of PRSS (Fig. 9(a4)) is lower than that of GRSS (Fig. 9(a3)). Although the PRSS makes some of the sensors out of the sensing area due to the layer structure, the coverage ratio of PRSS (Fig. 9(b4)) is higher than that of the other algorithms. By dividing the multiple layers and considering it a priority to make the sensor coverage reasonable, PRSS can cover the area effectively.

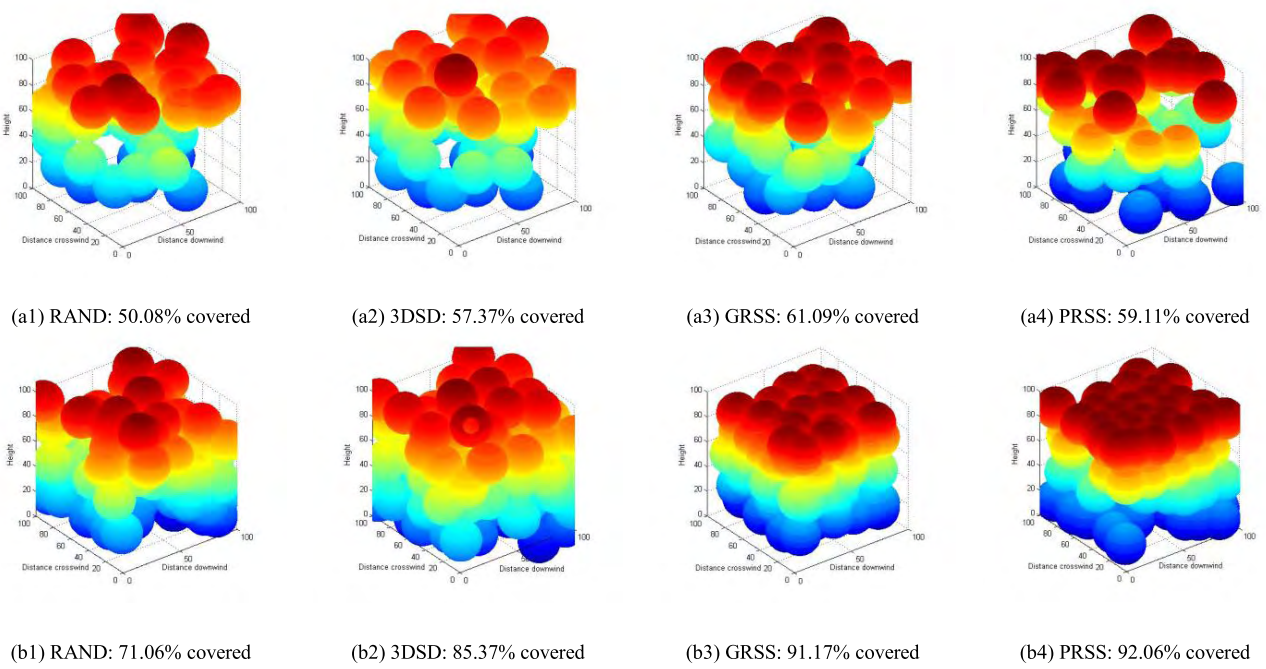

(a1) RAND: 50.08% covered (a2) 3DSD: 57.37% covered (a3) GRSS: 61.09% covered (a4) PRSS: 59.11% covered

(b1) RAND: 71.06% covered (b2) 3DSD: 85.37% covered (b3) GRSS: 91.17% covered (b4) PRSS: 92.06% covered

FIGURE 9. Sensor deployment status using the RAND, 3DSD, GRSS and PRSS algorithm at different initial configurations: (a1) 50 nodes using RAND; (a2) 50 nodes using 3DSD at the 50th round; (a3) 50 nodes using GRSS at the 50th round; (a4) 50 nodes using PRSS at the 50th round; (b1) 100 nodes using RAND; (b2) 100 nodes using 3DSD at the 100th rounds; (b3) 100 nodes using GRSS at the 100th round; (b4) 100 nodes using PRSS at the 100th round.

Fig. 10 displays the coverage under a different number of sensors using RAND, 3DSD, GRSS and PRSS at the 100th round. We observe that when we deployed the same number of sensors in the same area, when the number of sensors increases, the coverage ratios of the methods all increase and the proposed algorithms have better sensing coverage than the other algorithms. The average coverage ratio of GRSS is 21.65% higher than RAND and is 5.92% higher than 3DSD. The average coverage ratio of PRSS is 20.47% higher than RAND and is4.81% higher than 3DSD. The coverage ratios do not appear much different between the GRSS and PRSS. The average coverage ratio of GRSS is slightly higher than PRSS when the number of sensors is less than 80($\delta = 1.1310$). The reason is that the PRSS algorithm makes some of the sensors go out of the sensing area due to the layer structure. However, when the value of δ increases, the influences of the sensors out of the sensing area made by PRSS become small compared with the coverage ratio. On the other hand, due to the layer structure, the PRSS changes the 3D sensors redeployment problem into a 2D problem that can quickly reach the required sensing coverage. Thus, the average coverage ratio of PRSS is slightly higher than that of GRSS when the number of sensors is more than 80.

Fig. 11 displays the coverage of 100 sensors using the algorithms of RAND, 3DSD, GRSS and PRSS at different rounds. When the rounds increase, the coverage ratios of the methods all increase. We observe that the proposed algorithms have better sensing coverage than the other algorithms. When the number of rounds increases, the coverage ratio growths of all

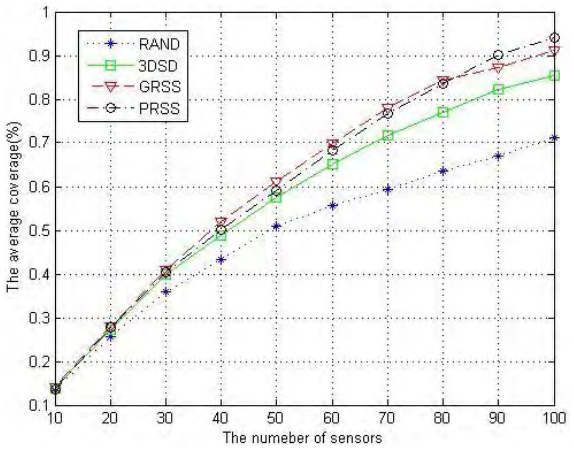

FIGURE 10. Comparisons of the average coverage while the number of sensors is increasing.

algorithms decline; however, the decline in the coverage ratio growth is higher for 3DSD than that for GRSS and PRSS. The reason is that the 3DSD makes some of the sensors go out of the sensing area due to a lack of boundary forces. On the other hand, due to the layer structure, PRSS changes the 3D sensors redeployment problem into four 2D problems in the simulation, which reaches the required sensing coverage more quickly than the GRSS. We also observe that the coverage ratios of all of the algorithms increase slightly after approximately 60 rounds because the sensor network will enter a stable state.

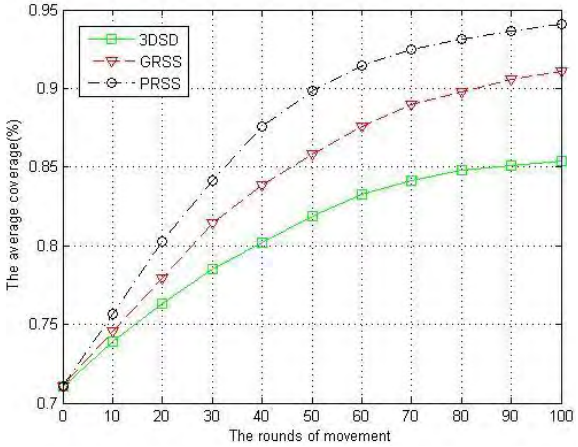

FIGURE 11. Comparison of the average coverage when the number of rounds increases.

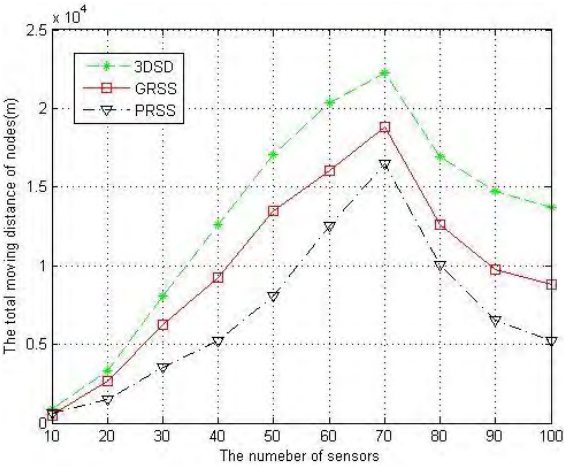

FIGURE 12. Comparisons of the average total distance while the number of sensors increases.

C. SIMULATION OF THE MOVING DISTANCE

Fig. 12 shows the total distances under different numbers of sensors using the algorithms of 3DSD, GRSS and PRSS at the 100th round. The total moving distances under our algorithms are shorter than those in the 3DSD algorithm. The reason is that the boundary forces are considered in our algorithms to reduce the unnecessary moving distances. The average total moving distance of GRSS is 26.71% less than that of 3DSD and that of PRSS is 47.50% less than that of 3DSD. Due to the layer structure, the 3D sensors redeployment problem in gas leakage monitoring is converted into multiple 2D redeployment problems, and the PRSS algorithm reduces the vertical movement distance and makes the movements of the sensors be more targeted. Thus, the average total movement distance of PRSS is 27.17% less than that of GRSS. When the number of sensors increases, the total distances of the three methods all increase, but they peak at the number 70 before starting to decline. The number of sensors is 70, and the value of δ is 0.9896≈1. The relationship $\delta < 1$ means

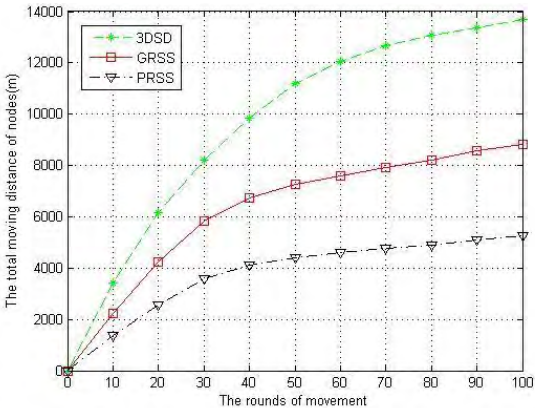

FIGURE 13. Comparisons of the average total distance when the number of rounds increases.

that the sensors are not sufficient to cover the monitoring area and the distance threshold between the two adjacent sensors is $r_i + r_j$. Thus, each sensor will move a far distance to cover the monitoring area as much as possible. On the other hand, the lower the number of sensors deployed in the same area, the shorter the total moving distance of the sensors is. In addition, the topology of the sensor network can reach stability easily and quickly. However, when the number of sensors is greater than 70 ($\delta > 1$), the distance threshold D_{ij} between two adjacent sensors becomes $(r_i + r_j)/\delta$. When the number of sensors increases, the value of δ also increases, but the distance threshold D_{ij} reduces. The distance threshold D_{ij} limits the movement distances of the sensors in each round in such a way that the total distances of the three methods begins to decrease.

Fig. 13 shows the total distances of the 100 sensors using the algorithms of 3DSD, GRSS and PRSS under different numbers of rounds. In Fig. 13, when the rounds increase, the average total distances of all of the algorithms all increase. However, the total moving distance of our algorithms are all shorter than the 3DSD algorithm at different rounds. The reason is that our algorithms consider the boundary forces to limit some of the sensors moving out of the boundary, and they reduce the unnecessary moving distances. The PRSS algorithm simplifies the 3D sensors redeployment problem and reduces the vertical movement distance of the sensors in such a way that the average total moving distance of GRSS is more than that of PRSS. It is easy to see that the average total distances of all of the algorithms all increase slightly after approximately 60 rounds because the sensors network tends to be stable.

D. SIMULATION OF THE ENERGY CONSUMPTION AND THE NETWORK LIFETIME

Fig. 14 shows a comparison of the average unit energy consumption under different numbers of sensors using the algorithms of 3DSD, GRSS and PRSS at the 100th round, and the sensors use RAND to be deployed at random. When the number of sensors increases, the average unit energy

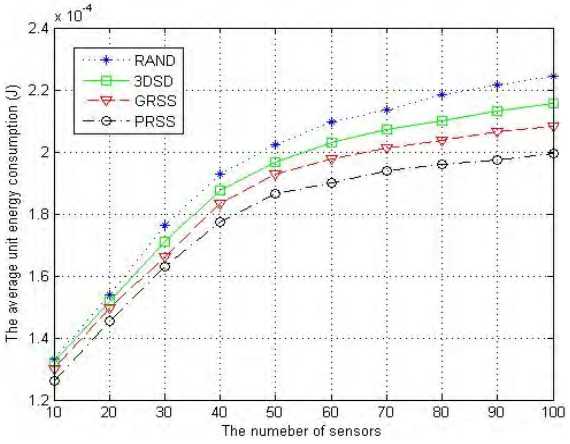

FIGURE 14. The comparisons of the average unit energy consumption with the number of sensors increasing.

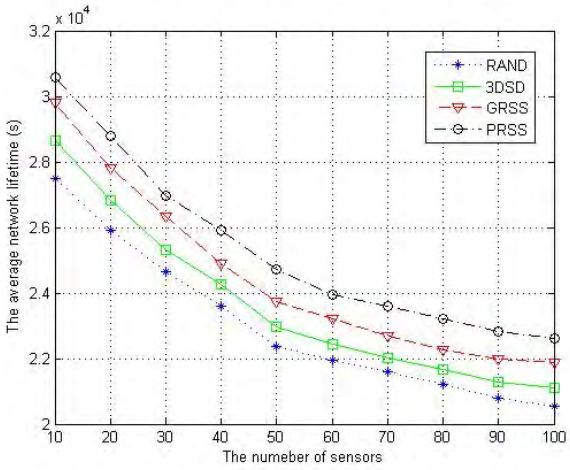

FIGURE 15. Comparisons of the average network lifetime when the number of sensors increases.

consumption also increases. We can observe that the average unit energy consumption of RAND is the highest in the four methods. The reason is that the sensor nodes are deployed irregularly, which requires more sensors to increase the hops to transfer the data. The average units of energy consumption of 3DSD is higher than that of GRSS and PRSS due to the lack of boundary forces. The average units of energy consumption of GRSS is 5.55% less than RAND and is 2.56% less than 3DSD. The average unit of energy consumption of PRSS is 9.34% less than RAND and is 6.23% less than 3DSD. The average units of energy consumption of GRSS is higher than PRSS due to the layer structure and the priority. This method makes the deployed sensors of PRSS be more focused than GRSS. Thus, the average units of energy consumption of PRSS is 3.58% less than that of GRSS. We also observe that the averages of the units of energy consumption of the four methods are all increasing slightly after the number of sensors is more than 60. The monitoring area and communication radius of the sensors are fixed in this simulation, and thus, the hops of the sensors that are close to the border do not change much when the number of sensors increases.

Fig. 15 shows a comparison of the average network lifetime under different numbers of sensors using the algorithms of 3DSD, GRSS and PRSS at the 100^{th} round, while the sensors to use RAND are deployed randomly. When the number of sensors increases, the average network lifetime decreases. The network lifetime is the time at which the first node dies in the WSNs. We can observe that the average network lifetime of RAND is the shortest among the four algorithms. The average network lifetime of GRSS is 6.23% longer than RAND, and the PRSS is 9.97% longer than RAND. The RAND method deploys the sensors irregularly, which requires more sensors to increase the hops to transfer data, to reduce the network life time. The average network lifetime of GRSS is 3.41% longer than 3DSD, and PRSS is 7.05% longer than 3DSD. The average network lifetime of 3DSD compared with RAND has improved because the sensor nodes that are deployed are relatively uniform. However, the 3DSD makes some of the sensors go out of the boundary and the hops of these sensors will be increased to transfer the data. Thus, the average network lifetime of 3DSD is shorter than that of GRSS and PRSS. The virtual sensing radius for the sink node is used in GRSS to balance the network node load and can increase the average network lifetime. The force of the sink in PRSS considers the surplus energy of its neighboring sensors to keep the sink away from low-power sensors. The sink in GRSS is fixed, and the ability to increase the average network lifetime is limited. Thus, the average network lifetime of GRSS is 3.52% shorter than PRSS.

VI. CONCLUSIONS

We presented a study of 3D virtual forces redeployment for mobile sensors in gas leakage monitoring. In this paper, the GRSS and PRSS redeployment algorithms are proposed to control the mobile sensors. To improve the coverage and make the movements of the sensors be targeted, the virtual boundary forces and the gas concentration are considered in the GRSS. To prolong the network lifetime, a virtual sensing radius is proposed for the sink to leave the neighboring sensors and move away when the surplus of energy in these sensors is low. To simplify the 3D redeployment problem, the monitoring area is divided into multiple layers and changes it into multiple 2D redeployment problems. We proposed the PSDL algorithm to redistribute the sensors among the layers according to their priorities. The layer priorities of the monitoring area are also considered in PRSS to make the monitoring of the sensors have pertinence. A virtual force method for the sink that considers the energy density is used in PRSS to prolong the network lifetime of the WSN. The simulation experiment shows that our algorithms improve the coverage, decrease the moving distance, reduce the energy consumption and prolong the network lifetime. In the future research, the multiple gas leak sources will be considered to redeploy the mobile sensors and monitor the accidents area.

REFERENCES

[1] A. Somov *et al.*, "Compact low power wireless gas sensor node with thermo compensation for ubiquitous deployment," *IEEE Trans. Ind. Informat.*, vol. 11, no. 6, pp. 1660–1670, Dec. 2015.

[2] L. Shu, M. Mukherjee, X. Xu, K. Wang, and X. Wu, "A survey on gas leakage source detection and boundary tracking with wireless sensor networks," *IEEE Access*, vol. 4, pp. 1700–1715, Jan. 2016.

[3] M. Cao, Q. Meng, Y. Wu, and M. Zeng, "Distributed sequential adaptive weighted localization of a gas-leakage source using a wireless sensor network," in *Proc. Chin. Control Decision Conf. (CCDC)*, Guiyang, China, 2013, pp. 3686–3691.

[4] X. Bian, Y. Zhang, Y. Li, X. Gong, and S. Jin, "A new method of using sensor arrays for gas leakage location based on correlation of the time-space domain of continuous ultrasound," *Sensors*, vol. 15, no. 4, pp. 8266–8283, Apr. 2015.

[5] A. Somov, A. Baranov, D. Spirjakin, and R. Passerone, "Circuit design and power consumption analysis of wireless gas sensor nodes: One-sensor versus two-sensor approach," *IEEE Sensors J.*, vol. 14, no. 6, pp. 2056–2063, Jun. 2014.

[6] A. Somov, A. Baranov, D. Spirjakin, A. Spirjakin, V. Sleptsov, and R. Passerone, "Deployment and evaluation of a wireless sensor network for methane leak detection," *Sens. Actuators A, Phys.*, vol. 202, pp. 217–225, Nov. 2013.

[7] A. Arfire, A. Marjovi, and A. Martinoli, "Model-based rendezvous calibration of mobile sensor networks for monitoring air quality," in *Proc. IEEE Sensors*, Busan, Korea, Nov. 2015, pp. 143–146.

[8] C. Chaiwatpongsakorn, M. Lu, T. C. Keener, and S. J. Khang, "The deployment of carbon monoxide wireless sensor network (CO-WSN) for ambient air monitoring," *Int. J. Environ. Res. Public Health*, vol. 11, no. 6, pp. 6246–6264, Jun. 2014.

[9] S. Grassini, M. Ishtaiwi, M. Parvis, and A. Vallan, "Design and deployment of low-cost plastic optical fiber sensors for gas monitoring," *Sensors*, vol. 15, no. 1, pp. 485–498, Dec. 2014.

[10] Y. Jiang, Z. He, Y. Li, Z. Xu, and J. Wei, "Weighted global artificial bee colony algorithm makes gas sensor deployment efficient," *Sensors*, vol. 16, no. 6, p. 888, Jun. 2016.

[11] H.-L. Fu, H.-C. Chen, and P. Lin, "Aps: Distributed air pollution sensing system on wireless sensor and robot networks," *Comput. Commun.*, vol. 35, no. 9, pp. 1141–1150, 2012.

[12] Z. Khalfallah, I. Fajjariy, N. Aitsaadiz, R. Langar, and G. Pujolle, "A new WSN deployment algorithm for water pollution monitoring in Amazon rainforest rivers," in *Proc. IEEE Global Commun. Conf. (GLOBECOM)*, Atlanta, GA, USA, Dec. 2013, pp. 267–273.

[13] Y. Guo, F. Kong, D. Zhu, A. Tosun, and Q. Deng, "Sensor placement for lifetime maximization in monitoring oil pipelines," in *Proc. 1st ACM/IEEE Int. Conf. Cyber-Phys. Syst.*, Stockholm, Sweden, Sep. 2010, pp. 61–68.

[14] H. P. Gupta, S. V. Rao, and V. Tamarapalli, "Analysis of stochastic K-coverage and connectivity in sensor networks with boundary deployment," *IEEE Trans. Intell. Transp. Syst.*, vol. 16, no. 4, pp. 1861–1871, Aug. 2015.

[15] Y. Zou and K. Chakrabarty, "Sensor deployment and target localization based on virtual forces," in *Proc. IEEE INFOCOM*, San Francisco, CA, USA, Apr. 2003, pp. 23059–23071.

[16] Y. C. Wang and Y. C. Tseng, "Distributed deployment schemes for mobile wireless sensor networks to ensure multilevel coverage," *IEEE Trans. Parallel Distrib. Syst.*, vol. 19, no. 9, pp. 1280–1294, Oct. 2008.

[17] G. Huang, D. Chen, and X. Liu, "A node deployment strategy for blindness avoiding in wireless sensor networks," *IEEE Commun. Lett.*, vol. 19, no. 6, pp. 1005–1008, Jun. 2015.

[18] T.-Y. Lin, H. A. Santoso, and K.-R. Wu, "Global sensor deployment and local coverage-aware recovery schemes for smart environments," *IEEE Trans. Mobile Comput.*, vol. 14, no. 7, pp. 1382–1396, Jul. 2015.

[19] F. M. Al-Turjman, H. S. Hassanein, and M. Ibnkahla, "Efficient deployment of wireless sensor networks targeting environment monitoring applications," *Comput. Commun.*, vol. 36, no. 2, pp. 135–148, Jan. 2013.

[20] T. Andersen and S. Tirthapura, "Wireless sensor deployment for 3D coverage with constraints," in *Proc. 9th Int. Conf. Netw. Sens. Syst. (INSS)*, Pittsburgh, PA, USA, 2009, pp. 1–4.

[21] S. Xiong, L. Yu, H. Shen, C. Wang, and W. Lu, "Efficient algorithms for sensor deployment and routing in sensor networks for network-structured environment monitoring," in *Proc. IEEE INFOCOM*, Mar. 2012, pp. 1008–1016.

[22] H. P. Gupta, S. V. Rao, and T. Venkatesh, "Analysis of stochastic coverage and connectivity in three-dimensional heterogeneous directional wireless sensor networks," *Pervasive Mobile Comput.*, vol. 29, pp. 38–56, Jul. 2016.

[23] S. M. N. Alam and Z. J. Haas, "Coverage and connectivity in three-dimensional networks with random node deployment," *Ad Hoc Netw.*, vol. 34, pp. 157–169, Nov. 2015.

[24] J. Huang, L. Sun, X. Wei, P. Sun, H. Huang, and R. Wang, "Redundancy model and boundary effects based coverage-enhancing algorithm for 3D underwater sensor networks," *Int. J. Distrib. Sensor Netw.*, vol. 10, no. 4, pp. 1–12, Apr. 2014.

[25] Z. Wang, B. Wang, and Z. Xiong, "A novel coverage algorithm based on 3D-Voronoi cell for underwater wireless sensor networks," in *Proc. Int. Conf. Wireless Commun. Signal Process. (WCSP)*, Nanjing, China, 2015, pp. 1–5.

[26] P. Jiang, S. Liu, J. Liu, F. Wu, and L. Zhang, "A depth-adjustment deployment algorithm based on two-dimensional convex hull and spanning tree for underwater wireless sensor networks," *Sensors*, vol. 16, no. 7, p. 1087, Jul. 2016.

[27] C. Zhang, X. Bai, J. Teng, D. Xuan, and W. Jia, "Constructing low-connectivity and full-coverage three dimensional sensor networks," *IEEE J. Sel. Areas Commun.*, vol. 28, no. 7, pp. 984–993, Sep. 2010.

[28] V. Nazarzehi and A. V. Savkin, "Decentralized control of mobile three-dimensional sensor networks for complete coverage self-deployment and forming specific shapes," in *Proc. IEEE Conf. Control Appl. (CCA)*, Oct. 2015, pp. 127–132.

[29] V. Nazarzehi, A. V. Savkin, and A. Baranzadeh, "Distributed 3D dynamic search coverage for mobile wireless sensor networks," *IEEE Commun. Lett.*, vol. 19, no. 4, pp. 633–636, Apr. 2015.

[30] C. Miao, G. Dai, X. Zhao, Z. Tang, and Q. Chen, "3D self-deployment algorithm in mobile wireless sensor networks," *Int. J. Distrib. Sensor Netw.*, vol. 11, no. 4, p. 721921, Apr. 2015.

[31] J. Lu and T. Suda, "Differentiated surveillance for static and random mobile sensor networks," *IEEE Trans. Wireless Commun.*, vol. 7, no. 11, pp. 4411–4423, Nov. 2008.

[32] E. Rashedi, H. Nezamabadi-Pour, and S. Saryazdi, "GSA: A gravitational search algorithm," *J. Inf. Sci.*, vol. 179, no. 13, pp. 2232–2248, 2009.

[33] C. Li and J. Zhou, "Parameters identification of hydraulic turbine governing system using improved gravitational search algorithm," *Energy Convers. Manage.*, vol. 52, no. 1, pp. 374–381, Jan. 2011.

[34] W. Meng, W. Xiao, L. Xie, and A. Pandharipande, "Diffusion based projection method for distributed source localization in wireless sensor networks," in *Proc. IEEE Conf. Comput. Commun. Workshops (INFOCOMWKSHPS)*, Apr. 2011, pp. 537–542.

[35] X. Liu and D. He, "Ant colony optimization with greedy migration mechanism for node deployment in wireless sensor networks," *J. Netw. Comput. Appl.*, vol. 39, pp. 310–318, Mar. 2014.

HE LI received the B.S. degree from the Shaanxi University of Science and Technology, Hanzhong, China, in 2010, and the M.S. degree from Henan Polytechnic University, Jiaozuo, China, in 2013. He is currently pursuing the Ph.D. degree with the State Key Laboratory of Networking and Switching Technology, Beijing University of Posts and Telecommunications, Beijing, China. His research interests include ad hoc and sensor network management.

YANG YANG received the Ph.D. degree from the Beijing University of Posts and Telecommunications. She was an Instructor with the Beijing University of Posts and Telecommunications in 2011. She holds a post-doctoral position with the University of Science and Technology Beijing. She is currently an Associate Professor with the State Key Laboratory of Networking and Switching Technology, Beijing University of Posts and Telecommunications. Her current research interests are cooperation and management in the MANETs.

XUESONG QIU was born in 1973. He received the Ph.D. degree from the Beijing University of Posts and Telecommunications, Beijing, China, in 2000. He is currently a Professor and the Ph.D. Supervisor with the State Key Laboratory of Networking and Switching Technology, Beijing University of Posts and Telecommunications. He has authored about 100 SCI/EI index papers. He presides over a series of key research projects on network and service management, including the projects supported by the National Natural Science Foundation and the National High-Tech Research and Development Program of China. He received 13 national and provincial scientific and technical awards, including the national scientific and technical awards (second-class) twice.

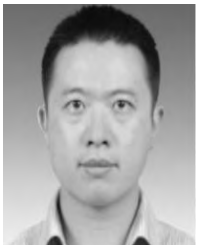

ZHIPENG GAO was born in 1980. He received the Ph.D. degree from the Beijing University of Posts and Telecommunications, Beijing, China, in 2007. He is currently a Professor and the Ph.D. Supervisor with the State Key Laboratory of Networking and Switching Technology, Beijing University of Posts and Telecommunications. He presides over a series of key research projects on network and service management, including the projects supported by the National Natural Science Foundation and the National High-Tech Research and Development Program of China. He received eight provincial scientific and technical awards.

GUIZHEN MA is currently pursuing the Ph.D. degree with the State Key Laboratory of Networking and Switching Technology, Beijing University of Posts and Telecommunications, Beijing, China. She is currently a Lecturer with the Tourism College of Beijing Union University. Her current research interest is fault management of wireless sensor networks.